

DEEP LEARNING CLASSIFIER OF LOCALLY ADVANCED RECTAL CANCER TREATMENT RESPONSE FROM ENDOSCOPY IMAGES

Jorge Tapias Gomez¹ Aneesh Rangnekar¹ Hannah Williams² Hannah Thompson²
Julio Garcia-Aguilar² Joshua Jesse Smith² Harini Veeraraghavan¹

¹ Department of Medical Physics, Memorial Sloan Kettering Cancer Center, USA

² Department of Surgery, Colorectal Service, Memorial Sloan Kettering Cancer Center, USA

ABSTRACT

We developed a deep learning classifier of rectal cancer response (tumor vs. no-tumor) to total neoadjuvant treatment (TNT) from endoscopic images acquired before, during, and following TNT. We further evaluated the network’s ability in a near out-of-distribution (OOD) problem to identify local regrowth (LR) from follow-up endoscopy images acquired several months to years after completing TNT. We addressed endoscopic image variability by using optimal mass transport-based image harmonization. We evaluated multiple training regularization schemes to study the ResNet-50 network’s indistribution and near-OOD generalization ability. Test time augmentation resulted in the most considerable accuracy improvement. Image harmonization resulted in slight accuracy improvement for the near-OOD cases. Our results suggest that off-the-shelf deep learning classifiers can detect rectal cancer from endoscopic images at various stages of therapy for surveillance.

Index Terms— Rectal cancer, endoscopy images, image harmonization, optimal mass transport.

1. INTRODUCTION AND RELATED WORKS

Endoscopy images acquired using flexible sigmoidoscopy is the standard-of-care technique for detecting cancer treatment response and early local regrowth in patients with locally advanced rectal cancer (LARC). However, clinical response assessment is highly variable [1] due to large variations in cancer appearance and varying degrees of response. Hence, we developed a deep learning-based approach to detect LARC response to total neoadjuvant therapy (TNT) at different time points, including pre-treatment (pre-Tx), during, and post-TNT. We also evaluated the zero-shot generalization when applying the network to detect new local regrowth (LR) occurring a few months to years following TNT. LR appears

different from pre-treatment tumors, constituting near out-of-distribution (OOD) data for classification.

Endoscopic images depict wide variations [2] due to scope positioning, occlusions, specular reflections, intensity saturation, presence of blood and stool, as well as telangiectasia occurring in response to radiation [3], thus presenting a challenge for achieving reliably accurate classification. Predominant prior methods focused on detecting and classifying precancerous lesions such as polyps in the lower gastrointestinal (GI) [4, 5] and peptic ulcers in the upper GI tract [6], as well as polyp segmentation [7, 8] through two broad approaches. The first class of methods employ a separate classifier to detect and mask out regions that reduce classification accuracy. The second approach used data-hungry transformer networks to extract more information from images [7–9]. Both approaches used several no-tumor images from endoscopy videos for analysis for improved robustness of artifacts.

Endoscopy videos are generally not stored as part of the standard of care. Videos have a higher proportion of no-tumor images, further exacerbating the class imbalance between no-tumor and tumor images, and introducing a different challenge. Finally, malignant cancers exhibit considerable heterogeneity and undergo appearance changes before and after treatment and at recurrence. Constraints of limited examples and variability of cancers motivated our approach that combines a non-deep-learning optimal transport (OT)-based harmonization [10] followed by off-the-shelf pretrained classifiers that are fine-tuned to the specific task. Prior work with retinal images has also shown that reducing imaging variations through harmonization [11] can improve accuracy.

Prior works have also addressed the issue of limited training examples using weakly supervised training [4], as well as synthesizing examples using generative adversarial networks [5], while using off-the-shelf deep learning architectures. An alternative approach to enhance generalization ability is through training regularization that includes data augmentation [12] and learning rate scheduling [13], which have been shown to improve performance with RGB images. We chose this latter training regularization approach

Jorge Tapias Gomez was an intern at Memorial Sloan Kettering Cancer Center during the project and contributed equally with Aneesh Rangnekar. Hannah Thomson performed this work when she was at Memorial Sloan Kettering Cancer Center.

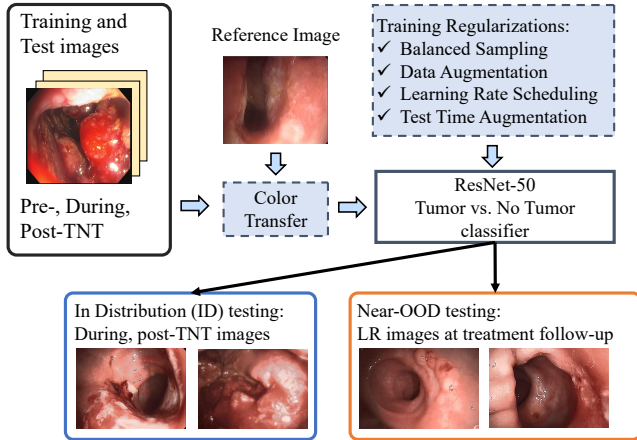


Fig. 1. Our endoscopy image analysis pipeline for automated detection of rectal cancer and response at various stages of cancer treatment. TNT: Total neoadjuvant therapy, LR: Local regrowth, OOD: Out-of-distribution.

to enhance the generalization capability of our classifier. In particular, we studied data augmentation (standard rotation, translation, scaling), balanced sampling, test time augmentation, and learning rate scheduling.

Our key contributions are (i) deep learning-based classification of rectal cancer treatment response during and following TNT as ID and near-OOD generalization assessment to detect new local regrowth at treatment follow-up from endoscopy images of patients with LARC and (ii) rigorous evaluation of the impact of training regularization and image intensity harmonization using a non-deep learning-based approach on ID and near-OOD test data.

2. METHODOLOGY

Fig. 1 depicts an overview of our approach. Endoscopy images are harmonized using an OT-based approach [10]. Harmonized images are input to a ResNet-50 [14] to generate the binary classification (tumor vs. no-tumor).

2.1. Image Harmonization via Optimal Transport

We addressed the challenge of endoscopy image intensity variations by employing a computationally efficient optimal transport (OT) based color intensity transfer approach to harmonize endoscopy images with respect to a selected reference image. The reference image was selected as the one devoid of tumor and free of artifacts (scope, light saturation) or other objects (blood, water bubbles, stool).

Concretely, our approach used an entropic regularization-based iterative convolution approach to approximate the 2-Wasserstein distance calculation. The intensity histogram of images was iteratively aligned with the reference histogram

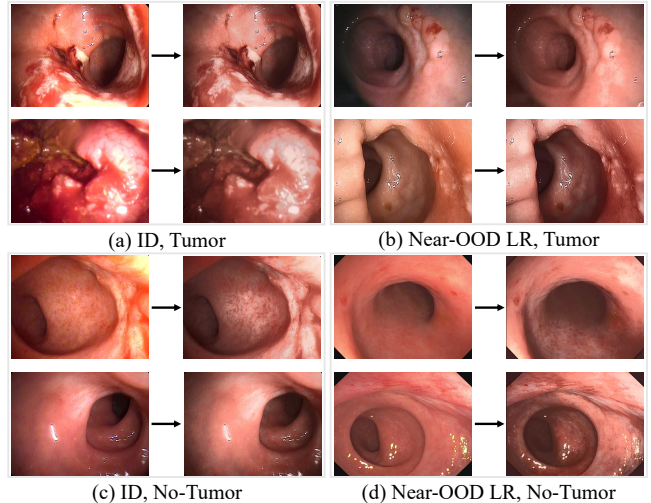


Fig. 2. Example images demonstrating OT-based image harmonization for four categories (original image \rightarrow converted image).

distribution (refer to [10] for detailed information on this process). For color transfer, we converted the RGB images into CIELAB color space and used the one-dimensional L (luminance) and two-dimensional ab (chrominance) as independent channels for image harmonization.

2.2. Regularization schemes

We explored several regularization techniques to enhance the performance of our final model:

- **Balanced sampling (BSA)** was performed during training to reduce the class imbalance between tumor and no-tumor samples within the mini-batches. BSA helped mitigate the challenge posed by continuously observing a single class through multiple mini-batch iterations.
- **Gradual warm-up or learning rate scheduling (LRS)** was adopted by setting the learning rate to a small value and gradually increasing it, as outlined in [13].
- **Data augmentations (DA)** consisted of random rotations in 90° steps, random horizontal flips, and random vertical flips, all of which were found to be effective for colonoscopy video analysis [12]. We also used the original images with none of the transformations above during the mini-batch to further augment the instances.
- **Test time augmentation (TTA)** was applied by generating three 90° rotation copies of each test image, followed by the generation of differently scaled versions for each copy (scaling parameters: 0.5, 0.7, 1.0, obtained via grid search). The final prediction was calculated by averaging the predictions from the individual images to provide an ensemble averaging that increased robustness to imaging differences.

2.3. Architecture details

We used ResNet-50 [14] as our primary network architecture and also evaluated on Wide Residual Network (Wide ResNet) [15] for ablation purposes. We initialized both networks with pretrained weights from ImageNet [16] and then fine-tuned them to generate binary classification (tumor vs no-tumor) from the endoscopy images. We replaced the networks’ fully connected layer with a linear layer (2048×2) for our classes. We trained multiple configurations using the earlier mentioned regularizations and with and without OT image harmonization.

2.4. Implementation Details

We harmonized all images to an expert-selected reference image for our experiments. The images varied in size from 568×424 pixels to 1920×1080 pixels. For training and evaluation, we resized all images to 224×224 pixels, as followed in ImageNet. We normalized the images using the ImageNet dataset mean and standard deviation, $[0.485, 0.456, 0.406]$ and $[0.229, 0.224, 0.225]$, respectively. All networks were trained for 50 epochs using a minibatch of 8, with a learning rate of $2e-5$, and the Adam optimizer with a linear weight decay of $1e-4$. When using LRS, we increased the learning rate from 0 to $2e-5$ within 10 epochs. We used Pytorch 1.13.1 with NVIDIA GPUs for all our experiments.

2.5. Datasets and metrics

We analyzed standard-of-care white light endoscopy images acquired from patients diagnosed with LARC who underwent total neoadjuvant therapy (TNT).

In-distribution (ID) dataset consisted of 2570 images (1329 with tumor and 1241 without visible tumor) acquired before treatment (Pre-Tx), during, and post-TNT. Fewer no-tumor examples resulted because we used only image snapshots in patients with surgeon-assessed complete response post-TNT. We trained all configurations using 1337 images (with 448 set aside for validation) and an ID test set of 785 images. Endoscopy videos are not routinely stored in our institution and are thus unavailable for analysis.

Near-OOD LR test data consisted of patients with LARC who initially responded to TNT and then placed on a watch and wait protocol, and followed every three months with imaging till a maximum of 3 years or when they developed LR. The dataset comprising 152 images (80 to LR and the rest to no visible tumor) was made available only after model training.

Metrics: Binary classifications were assessed by quantitatively evaluating key performance metrics, including accuracy, precision, and recall.

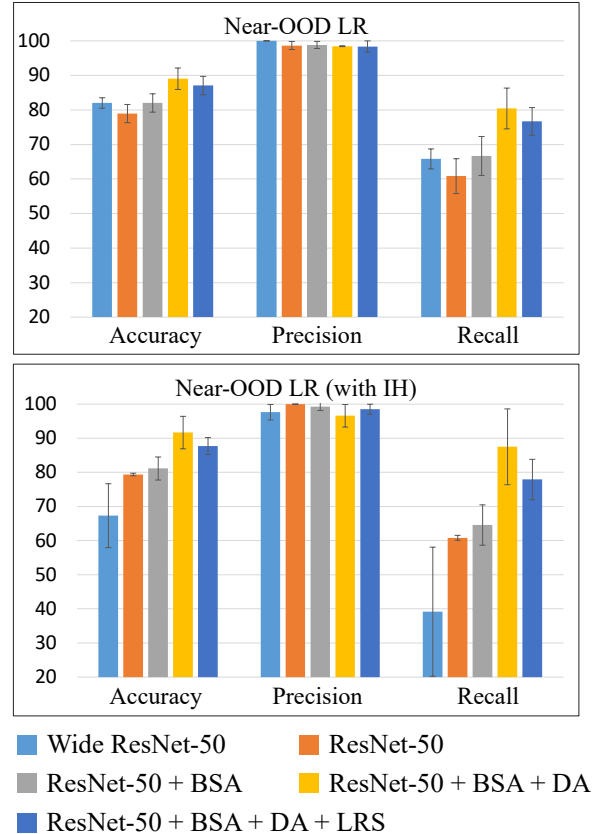


Fig. 3. Classifier accuracies comparing ResNet regularization variants and Wide ResNet, with and without IH.

3. RESULTS

Image harmonization Fig. 2 shows sample results of applying image harmonization using the OT method for both ID and LR examples. Despite blood, scars, and reflection from water bubbles, the OT method generated images with similar intensity-based appearance. Processing the OT color harmonization took 90 seconds to 120 seconds per image.

Classification performance on ID dataset without image harmonization As shown in Table. 1 Wide ResNet trained without image harmonization (IH) was more accurate than it’s IH-trained counterpart. ResNet50 with IH showed a small improvement in accuracy compared to the vanilla ResNet50. Incorporating additional training regularizations led to increased recall with ResNet50, even in the absence of IH. These findings suggest that the application of IH does not consistently enhance performance metrics on the ID data.

Impact of TTA TTA increased the accuracy of vanilla ResNet (ID: 88.96% \rightarrow 97.54%; LR: 74.56% \rightarrow 78.95%) and the ResNet trained with all the regularizations (ID: 91.04% \rightarrow 96.64%; LR: 76.32% \rightarrow 89.04%).

Classification performance on near-OOD (LR) dataset Fig. 3 illustrates the impact of various training regularizations

Table 1. Classification metrics on the ID dataset with IH (Image Harmonization), DA (Data Augmentation), BSA (Balanced Sampler), and LRS (Learning Rate Scheduling). We present the mean results from 3 runs with randomly initialized seeds. All reported numbers include test-time augmentation.

Model	Accuracy	Precision	Recall
ResNet-50	97.54	96.64	98.58
ResNet-50 + IH	98.05	98.00	98.16
ResNet-50 + BSA	97.28	95.44	99.41
ResNet-50 + BSA + DA	96.64	94.50	99.25
ResNet-50 + BSA + DA + LRS	94.65	90.80	99.67
ResNet-50 + BSA + DA + LRS + IH	93.12	88.87	99.16
Wide ResNet-50	98.60	99.07	98.15
Wide ResNet-50 + IH	94.27	97.95	90.62

Table 2. Intra/Inter-Cluster distances computed with t-SNE clustered embeddings for near-OOD and ID data points in ResNet trained with all the regularizations.

Cluster Distances	ID Train	ID Test	near-OOD LR
Intra Tumor	63.21 ± 11.83	49.77 ± 11.06	46.19 ± 22.10
Intra No-Tumor	24.52 ± 10.54	24.67 ± 14.71	15.56 ± 10.13
Inter	58.14	42.33	37.81

and image harmonization on the near-OOD or LR test set. Similar to the ID data, IH led to a larger reduction in the accuracy for the Wide ResNet. Conversely, the ResNet50 showed similar accuracy with and without IH. There was a small improvement in accuracy and recall when combining training regularizations with IH for the ResNet50, indicating a slight advantage when using IH. Balanced data sampling alone only resulted in a minimal accuracy improvement. However, combining balanced sampling with data augmentation resulted in the best accuracy for the ResNet50 independent of IH.

Analysis of difficulty in classifying near-OOD LR images

Fig.4 and Fig. 5 show the results of t-stochastic network embedding (t-SNE) [17] applied to ID and near-OOD or LR test datasets. As shown, the tumor and no-tumor samples are better separated when arising from the ID dataset compared to the near-OOD dataset. Representative image examples demonstrate the challenge in classification because the LR cases appear very similar to the no-tumor images. Table. 2 shows quantitative results of separability of near-OOD and ID cases computed as a distance of each sample with respect to its cluster centroid for intra- and to other cluster’s centroid for inter- distances. As shown, near-OOD samples had a smaller distance compared to ID samples, demonstrating the challenge in classifying LR (or tumor regrowth) from no tumor in the near-OOD images.

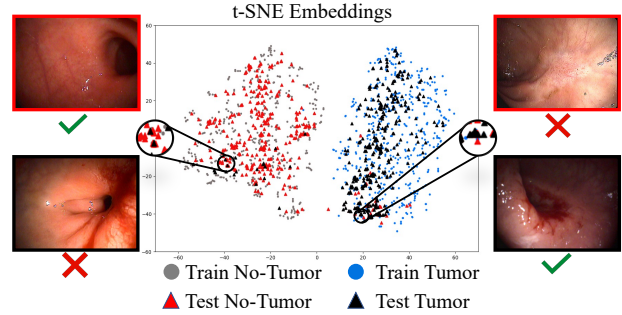


Fig. 4. t-SNE of ID (Train and Test) points, showing representative tumor and no-tumor images, with embeddings obtained from the ResNet trained with all the regularizations.

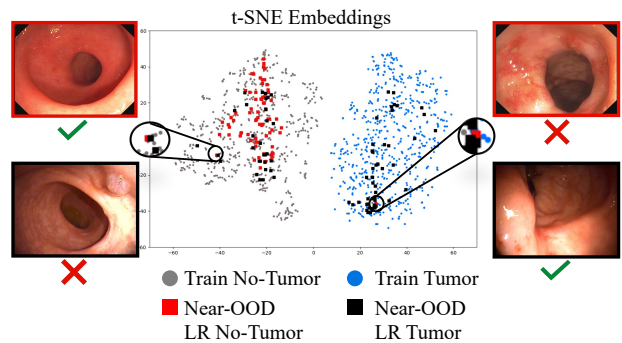


Fig. 5. t-SNE of ID Train and near-OOD LR data points, showing representative tumor and no-tumor images, with embeddings obtained from the ResNet trained with all the regularizations.

4. DISCUSSION AND CONCLUSION

We developed a deep learning classifier to distinguish tumor vs. no-tumor in endoscopy images taken at various stages of LARC treatment. Our analysis showed that test time augmentation was most effective in improving accuracy for ID and near-OOD datasets. Image harmonization slightly increased ResNet accuracy but reduced the Wide ResNet’s accuracy in near-OOD cases. Our paper is the first attempt to study how training regularization impacts the generalization capability of off-the-shelf deep learning classifiers in detecting malignant rectal cancers at different treatment and follow-up stages. Validation on larger multi-institutional cohorts, methods to further enhance the quality of endoscopy images, and domain generalization are future work.

5. COMPLIANCE WITH ETHICAL STANDARDS

This retrospective research study was conducted in line with the principles of the Declaration of Helsinki. Approval was granted by the Ethics Committee of Memorial Sloan Kettering Cancer Center.

6. ACKNOWLEDGEMENTS

This research was supported by Department of Surgery at Memorial Sloan Kettering. We thank Maria Widmar, Iris H Wei, Emmanouil P Pappou, Garrett M Nash, Martin R Weiser, and Philip B Paty, along with Hannah Thompson, Hannah Williams, Joshua Jesse Smith and Julio Garcia-Aguilar, for their assistance in collecting endoscopic images.

7. REFERENCES

- [1] S. Felder, S. Patil, E. Kennedy, and J. Garcia-Aguilar, "Endoscopic feature and response reproducibility in tumor assessment after neoadjuvant therapy for rectal adenocarcinoma," *Ann Surg Oncol*, vol. 28, no. 9, pp. 5205–5223, 2021.
- [2] S. Ali, M. Dmitrieva, N. Ghatwary, S. Bano, G. Polat, A. Temizel, A. Krenzer, A. Hekalo, Y. B. Guo, B. Matuszewski, M. Gridach, I. Voiculescu, V. Yoganand, A. Chavan, A. Raj, N. T. Nguyen, D. Q. Tran, L. D. Huynh, N. Boutry, S. Rezvy, H. Chen, Y. H. Choi, A. Subramanian, V. Balasubramanian, X. W. Gao, H. Hu, Y. Liao, D. Stoyanov, C. Daul, S. Realdon, R. Cannizzaro, D. Lamarque, T. Tran-Nguyen, A. Bailey, B. Braden, J. E. East, and J. Rittscher, "Deep learning for detection and segmentation of artefact and disease instances in gastrointestinal endoscopy," *Medical Image Analysis*, vol. 70, p. 102002, 2021.
- [3] H. Thompson, J. Kim, R. Jimenez-Rodriguez, J. Garcia-Aguilar, and H. Veeraraghavan, "Deep learning-based model for identifying tumors in endoscopic images from patients with locally advanced rectal cancer treated with total neoadjuvant therapy," *Dis Colon Rectum*, vol. 66, no. 3, pp. 383–391, 2023.
- [4] M. Yamada, Y. Saito, H. Imaoka, M. Saiko, S. Yamada, H. Kondo, H. Takamaru, T. Sakamoto, J. Sese, A. Kuchiba, T. Shibata, and R. Hamamoto, "Development of a real-time endoscopic image diagnosis support system using deep learning technology in colonoscopy," *Sci Rep*, no. 14465, 2019.
- [5] M. Turan and F. Durmus, "UC-NfNet: Deep learning-enabled assessment of ulcerative colitis from colonoscopy images," *Med Image Anal*, vol. 82, p. 102587, 2022.
- [6] Z. Dong, J. Wang, Y. Li, Y. Deng, W. Zhou, X. Zeng, D. Gong, J. Liu, J. Pan, R. Shang, Y. Xu, M. Xu, L. Zhang, M. Zhang, X. Tao, Y. Zhu, H. Du, Z. Lu, L. Yao, L. Wu, and H. Yu, "Explainable artificial intelligence incorporated with domain knowledge diagnosing early gastric neoplasms under white light endoscopy," *NPJ Digit Med*, vol. 6, no. 1, p. 64, 2023.
- [7] D.-P. Fan, G.-P. Ji, T. Zhou, G. Chen, H. Fu, J. Shen, and L. Shao, "Pranet: Parallel reverse attention network for polyp segmentation," in *Medical Image Computing and Computer Assisted Intervention – MICCAI 2020*, 2020, pp. 263–273.
- [8] B. Dong, W. Wang, D.-P. Fan, J. Li, H. Fu, and L. Shao, "Polyp-pvt: Polyp segmentation with pyramid vision transformers," *CAAI Artificial Intelligence Research*, vol. 2, p. 9150015, 2023.
- [9] N. Duc, N. Oanh, N. Thuy, T. Triet, and V. Dinh, "Colonformer: An efficient transformer based method for colon polyp segmentation," *IEEE Access*, vol. 10, pp. 80 575–80 586, 2022.
- [10] J. Solomon, F. de Goes, G. Peyré, M. Cuturi, A. Butscher, A. Nguyen, T. Du, and L. Guibas, "Convolutional wasserstein distances: Efficient optimal transportation on geometric domains," *ACM Trans. Graph.*, vol. 34, no. 4, 2015.
- [11] A. Subramaniam, F. Orge, M. Douglass, B. Can, G. Monteoliva, E. Fried, V. Schbib, G. Saidman, B. Peña, S. Ulacia, P. Acevedo, A. Rollins, and W. D.L., "Image harmonization and deep learning automated classification of plus disease in retinopathy of prematurity," *J Med Imaging (Bellingham)*, vol. 10, no. 6, p. 061107, 2023.
- [12] S. Ramesh, V. Srivastav, D. Alapatt, T. Yu, A. Murali, L. Sestini, C. I. Nwoye, I. Hamoud, S. Sharma, A. Fleurentin, G. Exarchakis, A. Karargyris, and N. Padoy, "Dissecting self-supervised learning methods for surgical computer vision," 2023.
- [13] P. Goyal, P. Dollár, R. Girshick, P. Noordhuis, L. Wesolowski, A. Kyrola, A. Tulloch, Y. Jia, and K. He, "Accurate, large minibatch sgd: Training imagenet in 1 hour," 2018.
- [14] K. He, X. Zhang, S. Ren, and J. Sun, "Deep residual learning for image recognition," 2015.
- [15] S. Zagoruyko and N. Komodakis, "Wide residual networks," in *Proceedings of the British Machine Vision Conference 2016, BMVC 2016, York, UK, September 19-22, 2016*. BMVA Press, 2016.
- [16] J. Deng, W. Dong, R. Socher, L.-J. Li, K. Li, and L. Fei-Fei, "Imagenet: A large-scale hierarchical image database," in *2009 IEEE Conference on Computer Vision and Pattern Recognition*, 2009, pp. 248–255.
- [17] L. Van der Maaten and G. Hinton, "Visualizing data using t-sne." *Journal of machine learning research*, vol. 9, no. 11, 2008.